PERFORMANCE-BASED DESIGN WITH LIFE-CYCLE COST ASSESSMENT FOR DAMPING SYSTEMS INTEGRATED IN WIND EXCITED TALL BUILDINGS

Laura Micheli, Alice Alipour, Simon Laflamme, Partha Sarkar

Abstract

The application of performance-based design (PBD) is gaining increasing interest in the wind engineering community. A popular design approach to minimize wind induced vibrations in flexible civil structures is to size structural stiffness and supplemental damping systems in order to restrict the motion to a given threshold for providing safety and comfort, while ensuring that structural components meet strength requirements. In this paper the PBD paradigm is extended to wind excited tall buildings equipped with motion control systems. The objective is to improve the design of damping systems under different wind events while considering maximum acceleration as performance measure. In addition, since the installation of damping devices implies additional costs (e.g., installation and maintenance costs) while it helps decreasing the costs associated with performance failure, a life-cycle analysis (LCA) is integrated in the PBD. In the LCA framework, the percentage of building occupants affected by discomfort and motion sickness caused by excessive wind-induced vibrations is considered to account for the consequences of different target performance levels. The developed PBD is applied to a 39-story building that has documented issues with excessive vibrations under wind events. The wind load is simulated as a multivariate stochastic process, in the time domain. Two passive vibration mitigation strategies are investigated: viscous and friction dampers, both designed to meet the target performance levels. LCA are conducted for the building equipped with each damper type, and benchmarked against the one without dampers. Results show that the PBD leads to a rational and economically effective approach for the design of the damping systems in wind excited tall buildings.

1. Introduction

Performance-based design (PBD) has shown to be an effective philosophy to create risk consistent designs within the seismic engineering community (Moehle and Deierlein 2004, Yang *et al.* 2009, Federal Emergency Management Agency 2012). In the past years, numerous attempts have been made to extend the application of PBD to other hazards such as wind load (Van de Lindt and Dao 2009, Ciampoli and Petrini 2011, Spence and Kareem 2014), fire (Liew et al. 2002), corrosion (Biondini and Frangopol 2009), and seismic pounding (Tubaldi et al. 2012). In wind engineering,

many of the proposed PBD procedures have been devoted to tall buildings, with particular focus on the serviceability limit states (Petrini and Ciampoli 2012, Spence and Gioffre 2012, Bernardini *et al.* 2014). The use of passive supplemental energy damping systems to improve the performance of high-rise structures under wind load is now widely accepted (Kareem *et al.* 1999, Saaed *et al.* 2015). However, a PBD methodology that integrates the design of passive damping systems in a tall building has yet to be developed. In motion engineering, the idea of PBD is to minimize structural vibrations by appropriately sizing supplemental damping systems in order to restrict the motion to a given threshold for providing safety and comfort, while designing the structural stiffness to ensure that structural components meet strength requirements (Connor and Laflamme 2014). This requires the development of a PBD procedure for tall buildings that includes the design of the motion control devices.

Passive damping systems, such as tuned-mass damping, viscous damping, and base-isolation, are widely used to enhance the structural performance under natural hazards. Some of the attractive features of this technology are the high reliability of the devices, the robustness against possible mechanical failures, and their inherent stability. In the wind hazard case, passive damping systems are generally designed for a predominant wind speed, without considering temporal and spatial variations of the wind load throughout the life span of the structure (McNamara *et al*. 2000, Moon 2010, Laflamme *et al.* 2012). The use of nonlinear damping devices, such as friction elements, further complicates the analysis, because the computation of equivalent damping depends highly on the excitation itself (Cao *et al.* 2016). These factors should be considered to improve existing design procedures, in order to provide a rational and economically effective design of the damping system.

The financial benefits of supplemental damping systems for wind-induced vibration mitigation has been the topic of ample research. In the literature, three types of cost-evaluation strategies concerning wind load and damping devices can be found. In the first type, only the initial cost of the device is included in the cost analysis and the total cost of the controlled building is compared against an alternative strategy, such as increase of structural stiffness in the uncontrolled structure or another control system (Jackson *et al.* 2010, Laflamme 2011). The second type involves a cost-based optimization procedure, in which a tuned mass damper is designed to guarantee the building occupants' comfort under a certain wind speed (Tse *et al.* 2012, Li and Hu 2014, Wang *et al.* 2016). Finally, some studies have focused on the estimation of the life-cycle cost (LCC) of tall

buildings subjected to wind excitation without auxiliary damping devices. The wind induced-damage is usually related to lateral drift limitations and intervention costs of nonstructural elements (Cui and Caracoglia 2015, Ierimonti *et al.* 2017, Chuang and Spence 2017). While some of these studies are important steps towards providing financial justifications for the implementation of motion control systems for improving structural resilience versus wind, none of the studies considered the variability of the excitation or the uncertainty in the damper response under different wind loads, and the life-cycle savings arising from wind-induced vibration suppression. In addition, the wind-induced damage is related to repair and replacement costs of nonstructural elements, and few attention is given to the indirect economic losses in business activities associated with the building occupants' discomfort.

Recent research demonstrated that excessive wind-induced vibrations may lead to a relevant loss in work productivity of the building occupants' (Lamb *et al.* 2014, Lamb and Kwok 2016, Lamb and Kwok 2017). Wind-induced vibrations generate motion sickness, sopite syndrome, and other adverse effects, including fear, nausea, and drowsiness. Excessive accelerations can interfere with the building inhabitants' daily operations, affecting their well-being and creating an uncomfortable environment. Surveys reported in literature show that in some cases wind-induced vibrations generated difficulty in walking, while there are other cases in which employees presented motion sickness symptoms and were dismissed from their job activities (Kwok *et al.* 2009, Burton *et al.* 2015). All these studies demonstrate that the indirect costs associated with the building occupants' discomfort and business downtime caused by wind-induced vibrations in high-rise structures should not be neglected. Therefore the life-cycle cost model needs to account for such losses.

The goal of this paper is to provide an economically effective design procedure for damper devices, in order to extend the application of the PBD paradigm to passive damping systems integrated in tall buildings. In the proposed PBD procedure, performance requirements in terms of maximum acceptable accelerations are introduced and characterized with different mean wind speed and recurrence intervals. A life-cycle analysis (LCA) is embedded in the procedure to financially quantify the effectiveness of the motion devices. The LCA utilizes the concept of vulnerability analysis to estimate the indirect costs associated with building occupants' discomfort over the lifetime of the structure. The LCA provides a robust tool to estimate the effectiveness of the damping system and justify its initial investment.

The paper is organized as follows: Section 2 draws a general background regarding PBD and acceleration thresholds. Section 3 discusses the adapted PBD philosophy for design of passive damping devices under wind, introduces performance objectives, wind hazard levels, and life-cycle analysis. Section 4 explains the building and wind simulation techniques. Section 5 presents the application of the proposed approach to an existing 39-storey building, located in Boston, and equipped with viscous and friction dampers. Section 6 discusses the conclusions and possible future directions for research.

2. Background

2.1 Performance-based design

The PBD methodology relies on the definition of target system performance levels associated with different hazard intensities. In earthquake engineering, four different target performance levels are defined: fully operational, operational, life safety, and near collapse. These states are associated with frequent, occasional, rare, and very rare design loads. The designer chooses a combination of target performance and hazard levels as the design objective, depending on various parameters including the usage type, expected performance after hazard, and expected repair costs (Porter 2003). An intensity measure is selected to characterize the external hazard and the system target performance level is related to engineering demand parameters (EDP), such as drift, acceleration, and ductility. To estimate the target performance level, maximum acceptable values are selected for the EDPs as thresholds and compared with the structural response. Therefore, a PBD framework requires the definition of hazard levels, the selection of appropriate building EDPs and the consequences of exceeding the defined target performance levels.

These information can be used to conduct a life-cycle analysis (LCA). LCA is a powerful tool that allows to compute all the costs from construction to the end of the structure's life span. More specifically, the total life-cycle cost (LCC) can be estimated as the sum of the current value of construction cost, inspection and maintenance costs and serviceability failure costs adjusted to future values (Wen and Kang 2001). Generally, the initial cost of construction is considered constant, the inspection and maintenance costs depend on the maintenance strategy adopted and increase with the age of the structure, while the serviceability failure costs vary over a prefixed period of time (usually, the design life of structure). Failure costs are often described as the costs associated with repair and replacement of the damaged components after a hazard event.

The focus of this study is on wind excitations and the failure costs are based on the user costs corresponding to the building occupants discomfort and motion-sickness. Sec. 2.2 discusses the acceleration limitations and recommendations for human comfort in high-rise structures.

2.2 Acceleration Thresholds

Tall buildings are light, slender structures, characterized by low natural frequencies and low inherent damping, and therefore very sensitive to wind excitation. The wind flow acting on a high-rise structure can generate turbulence buffeting and vortex shedding, responsible for low frequency vibrations. The vibrations induced by these wind effects may adversely affect the building occupants. The motion of the building may induce motion sickness, which arises at low frequency of vibration (e.g., range 0.1 to 1 Hz). Low persistent acceleration levels can generate sopite syndrome, characterized by sleepiness, low mood and loss in concentration. Other effects, such as fear, nausea, and drowsiness contribute to the creation of an uncomfortable environment, in both office and residential buildings.

The mechanism of perceiving and responding to motion is a very complex process of the human body, which results from physiological and psychological reactions to motion exposure. Many parameters, such as the occupant expectation, the activity, the body position, the exposure duration, and the presence of motion cues influence the motion perception mechanism. In addition, the human response to motion is personal, and it may vary from an individual to another. The subjectivity of the motion perception is one of the main challenges to the establishment of common accepted acceleration tolerance thresholds for the serviceability design of high-rise structures.

Acceptance criteria for wind-induced motion of tall buildings have been published in some international and national standards. For instance, the Architectural Institute of Japan (2004) introduced serviceability guidelines based on the proportion of building occupants' that will likely perceive the motion, as function of the first natural frequency of the structure. Based on these specifications, the annual maximum acceptable accelerations vary between a minimum of 1 mg to a maximum of 20 mg, depending on the natural frequency of the building. Tamura *et al.* (2006) proposed probabilistic perception thresholds for the habitability design of tall buildings. The acceleration thresholds range between 0.4 mg and 30 mg, depending on the percentage of building inhabitants that will perceive the motion and the natural building frequency. Kwok *et al.* (2015) defined three acceleration thresholds including motion perception (peak acceleration $\geq$ 5 mg),

where only some occupants can perceive the motion and rarely create alarm; comfort level (peak acceleration ≥ 10 mg), where the majority of the building occupants' feel the motion; fear (peak acceleration ≥ 35-40 mg), where alarm and lose balance are common. The inclusion of different response levels in Kwok *et al.* (2015) represents an enhancement in comparison with other standards. However, all these criteria are based on experimental studies performed in motion simulators, under prescribed conditions. In actual applications in North America it is common practice to assume 10-15 mg for residential buildings and 20-25 mg as peak acceleration target for office buildings, as reported in Kareem *et al.* (1999) and McNamara *et al.* (2003). Further multi-disciplinary research is needed to gain a better understanding of human behavior and motion thresholds in wind-excited high-rise buildings (Lamb and Kwok 2017).

3. MOTION PERFORMANCE BASED-DESIGN

3.1 Proposed PBD Procedure

In this paper, the peak acceleration experienced by the building, a_{peak}, is taken as EDP to identify the performance levels. The mean hourly wind speed at height of interest $V_{m,z}$ (e.g., z = height of the building) is selected as intensity measure. This is a common choice in wind-based PBD, being a site-specific measure readily available through analysis of meteorological data (Spence and Kareem 2014, Chuang and Spence 2017). The focus of this study is on four levels of wind hazard events, representative of very frequent, frequent, occasional, and rare scenarios. The following mean recurrence intervals (MRI) of the wind speed are considered: 1, 10, 50 and 100 years. They correspond to a probability of exceedance of 1.00, 0.99, 0.63 and 0.39 in 50 years (assumed as design life of the structure). Note that in the majority of the PBD procedures for wind excited buildings the rare wind event is taken as the 475 or 700 years MRI event (Burns 2002, Griffis *et al*. 2013, Huang *et al*. 2015). Since the objective of the proposed PBD is the acceleration control, the 100 years MRI is considered as a rare event, assuming that during a very rare event (e.g., hurricane, tornado) the acceleration control is usually not the major issue.

For each wind hazard level, a maximum acceptable peak acceleration range is defined, as shown in Fig. 1. Ranges are selected instead of single thresholds because, as shown in Sec. 2.2, there is no common agreement in the acceleration values that trigger motion perception or motion sickness. The proposed PBD (Fig. 1) includes three performance objectives: basic, essential and critical. The basic line is the basic design objective that the majority of the buildings should satisfy. For instance, the maximum acceleration experienced by a structure should be between 10 mg and 25

mg for the negligible limit state under the very frequent wind level (MRI = 1 year). The essential line is based on a more restrictive criterion. For instance, it may be the objective of a research laboratory with sensitive equipment. The critical objective is the most precautionary and motion restrictive objective. The critical performance is in place for buildings that must remain fully operational during rare wind events. Examples of such buildings include hospitals and strategic governmental buildings. The acceleration thresholds related to different performance objectives vary as the wind hazard level increases. As an example, the medium acceleration threshold (35-45 mg) is acceptable under the basic performance objective for occasional winds (50 years MRI). Depending on the design requirements, the PBD may contain a combination of acceleration and drift limitations. However, in high-rise structures designing the dampers to restrain the peak accelerations is usually more efficient than designing for displacements.

Once the performance objective is selected, the damping ratio, the number and the capacity of the damping devices is designed. The design process is schematized in the flow chart in Fig. 2. A numerical simulation in the time domain is conducted for each wind hazard level and the maximum acceleration experienced from the building recorded. Then, the maximum acceleration is compared with the corresponding acceleration thresholds. If the peak acceleration is lower than the acceleration threshold for all wind hazard levels, the probability of failure of the structure can be calculated through conditional probability functions. Otherwise, the dampers have to be re-designed iteratively until the target performance is achieved. The probability of failure of the structure can be used in conjunction with the annual probability of occurrence of the wind speed to evaluate the annual failure costs associated with the exceedance of one or more acceleration ranges. Note that the proposed approach could be used also when a more complex version of the limit state condition is assumed. For instance, one could weigh the acceleration thresholds with the frequency of the building, identifying the corresponding acceleration limitations through available charts or equations (such as those in Architectural Institute of Japan 2004). In such case, the acceleration thresholds reported in Fig. 1 would be replaced with the frequency-dependent limits, and the dampers designed under the four different wind hazard levels, as outlined in the above described procedure.

Next section describes the method used to estimate the economic losses associated with the exceeding of the acceleration ranges.

3.2 Life-cycle analysis

The total LCC of a structure equipped with damping devices can be obtained using (Alipour *et al.* 2010):

$$LCC = C_0 + C_I + C_m + C_f \tag{1}$$

where C_0 is the initial construction cost of the building, C_I is the installation cost of the dampers, C_m denotes the maintenance cost for the dampers and the structure, and C_f represents the cost of failure, expressed as:

$$C_f = \sum_{i=1}^{N_t} \sum_{j=1}^{k} C_j P_j (1+r)^{-i\Delta t} \tag{2}$$

where Δt is the time interval (taken as 1 year), N_t is the number of time periods considered (equal to the design life of the structure), r represents the expected return rate (taken as 5%), k is the number of performance levels considered (equal to 4), P_j denotes the probability of the j-th performance level threshold being exceeded, and C_j is the monetary loss associated with the j-th performance level threshold being exceeded.

The probability of exceedance of the j-th acceleration threshold P_j, can be defined as:

$$P_j = \int_{V_{m,z,\min}}^{V_{m,z,\max}} F_j\left(V_{m,z}\right) f\left(V_{m,z}\right) \mathrm{d}V_{m,z} \tag{3}$$

where $V_{m,z}$ is the mean hourly wind speed at the height of interest z, ranging between $V_{m,z,\min}$ and $V_{m,z,\max}$, $F_j\left(V_{m,z}\right)$ denotes the probability of failure to meet the j-th acceleration threshold, conditional to the occurrence of $V_{m,z}$, while $f\left(V_{m,z}\right)$ represents the annual probability of exceedance of $V_{m,z}$ (extracted from the hazard curve), that is specific to the building site. In general, $V_{m,z,\min}$ and $V_{m,z,\max}$ can be viewed as the range of wind speeds that the structure will experience during its life. The detailed procedures for the estimation of $F_j\left(V_{m,z}\right)$ and $f\left(V_{m,z}\right)$ for the case study building are given in Sec. 5.4.

Finally, the cost C_j in Eq. (2) is related to the indirect costs corresponding to the adverse effects of the wind-induced accelerations on the building inhabitants (e.g., general discomfort, sopite

syndrome and motion-sickness). To estimate the expected acceleration costs the following assumptions are made:

i. It is assumed that 5.4 % of the employees working on the top third of the building are affected from sopite syndrome or motion sickness when the maximum floor acceleration exceeds the negligible limit state (peak acceleration >10 mg), with a consequent mean loss in productivity of 30 % per person (Lamb and Kwok 2016).

ii. The average annual salary of the single employee is estimated as US$112,500 (National occupational employment and wage estimates united states, 2015). Assuming 235 workdays per year for each employee, the average daily salary is taken as US$477 (corresponding to managerial positions, usually located at top floors of the tall building).

iii. It is assumed that higher levels of acceleration correspond to higher percentages of building occupants affected by motion sicknesses, while maintaining the loss of work productivity at 30 %.

iv. It is assumed that, in all the cases, the wind-induced motion is felt once a month (12 times/year) (Lamb et al. 2014).

From *i* and *ii* the loss in productivity of each employee can be estimated as C_A = US$143/day. Therefore, C_j can be expressed as:

$$C_j = C_A \, \rho_p(\%) N_E N_A \tag{4}$$

where ρ_p is the percentage of building occupants affected by motion discomfort, N_A is the annual number of times in which the wind-induced motion is experienced (N_A = 12 from *iv*), and N_E is the number of employee located on the top third floors of the building (N_E is estimated based on standard office floor plan). To the best of the authors' knowledge an empirical or analytical relationship between percentage of building occupants affected by motion discomfort, ρ_p, and the peak floor acceleration, a_{peak}, is not available. For this purpose, this paper examines the adoption of four different relationships between ρ_p and a_{peak}: two linear, a concave and a convex function. More details on these ρ_p - a_{peak} relationships are discussed in Sec. 5.3.

The LCC of the building equipped with the motion control system can be used as a metric for the damper effectiveness. Such metric could be utilized for financially justifying the installation of a damping system enabling a lighter structural system, or to compare different control solutions. It

could be, for example, employed for the selection of a set of viscous dampers or a tuned mass damper. If the LCC is not acceptable, the damper design can be iteratively modified.

To perform the PBD, the structural response of the building under different wind load intensities needs to be estimated. The next section discusses the techniques used to numerically simulate the building response and the wind speed.

4. SIMULATION METHODS

4.1 Simulation of Building Response

The structure is modeled using the state-space formulation. The equation of motion for an *n*-degree-of-freedom (DOF) building can be written as:

$$\mathbf{M}\ddot{\mathbf{x}} + \mathbf{C}\dot{\mathbf{x}} + \mathbf{K}\mathbf{x} = \mathbf{E}_w\mathbf{w} - \mathbf{E}_u\mathbf{u} \tag{5}$$

where **M**, **C**, and **K** are square matrices of dimension $n \times n$ representing the system's mass, damping and stiffness, respectively, **x** = $n \times 1$ the displacement vector, **w** = $n \times 1$ the vector containing the external excitation (wind load), **u** = $q \times 1$ the control force vector, $\mathbf{E}_w = n \times n$ the input location matrix for the load, $\mathbf{E}_u = n \times q$ the input location matrix for the control force, q the number of controlled floors, and n is taken as the number of floors for a structure simulated in a single direction. The state space model is written:

$$\dot{\mathbf{X}} = \mathbf{A}\mathbf{X} + \mathbf{B}_w\mathbf{w} - \mathbf{B}_u\mathbf{u} \tag{6}$$

where $\mathbf{X} = [\mathbf{x}\ \dot{\mathbf{x}}]^T$ is the $2n \times 1$ state vector and **A**, $\mathbf{B}_u$ and $\mathbf{B}_w$ are expressed:

$$\mathbf{A} = \begin{bmatrix} \mathbf{0} & \mathbf{I} \\ -\mathbf{M}^{-1}\mathbf{K} & -\mathbf{M}^{-1}\mathbf{C} \end{bmatrix}_{2n \times 2n} \tag{7}$$

$$\mathbf{B}_u = \begin{bmatrix} \mathbf{0} \\ \mathbf{M}^{-1}\mathbf{E}_u \end{bmatrix}_{2\mathrm{n} \times \mathrm{q}} \tag{8}$$

$$\mathbf{B}_w = \begin{bmatrix} \mathbf{0} \\ \mathbf{M}^{-1}\mathbf{E}_w \end{bmatrix}_{2n \times n} \tag{9}$$

4.2 Wind Load Simulation

In this study, the wind load is simulated in the time domain. The time integration is necessary due to the nonlinear dynamic behavior of the employed damping system. If the system was linear, including the passive dampers, the response could have been obtained in the frequency domain

using transfer functions. The wind load vector **w** in Eq. (6) consists of the along wind fluctuating forces acting on the floors in the simulated direction. At floor *j*, the wind load is expressed as:

$$F_j(t) = \rho\, C_D A_j V_{m,j} V_{t,j}(t) \tag{10}$$

where ρ is the air density, C_D is the drag coefficient (dependent on the building shape), and A_j is the projected frontal area of the building normal to the wind flow at the *j*-th floor, $V_{m,j}$ is the mean component of the wind speed at the *j*-th floor, and $V_{t,j}(t)$ is the fluctuating component of the wind velocity at the *j*-th floor. The fluctuating $V_{t,j}(t)$ is generated by the wind turbulence and it is simulated using the spectral approach described in Appendix A. This approach has been selected because it showed high accuracy in wind time histories simulation (Ubertini and Giuliano 2010, Tamura and Kareem 2013). Furthermore, the spectral approach could be used also to simulate the wind speed acting on the across wind direction, as reported in Ref. (Rossi *et al.* 2004, Tamura and Kareem 2013, Hou and Sarkar 2018).

5. APPLICATION OF THE PBD METHODOLOGY ON A CASE STUDY BUILDING

In this Section, the proposed methodology is applied to an existing 163 m 39-story office tower located in Boston, Massachusetts. The building is a steel moment-frame tube system of octagonal plan layout. Previous studies demonstrated that the uncontrolled structure experienced high acceleration levels, in the order of 40 – 70 mg for the frequent wind hazard level (McNamara *et al.* 2000, McNamara and Taylor 2003). These high accelerations were attributed to the vortex shedding caused by an adjacent building. In order to reduce the wind-induced vibrations, the building was equipped with a supplemental damping system and with toggle braces, which are used to increase the performance of the damping system. The supplemental damping system consists of a set of two viscous dampers installed at every other floor, starting from the 5th floor up to the 33th, for a total of 30 dampers. The actual viscous control strategy provides an additional damping of 2% (McNamara and Taylor 2003). Fig. 3 is a schematic representation of the building elevation on its simulated axis, along with the wind load profile, showing the viscous dampers in blue. The number of controlled floors is q = 15. Note that the direction where the acceleration are largest is simulated, and that the building does not present torsional effects or coupled modes (McNamara *et al.* 2000). Furthermore, the last three floors of the structure are not occupied, therefore only the first 36 floors are considered in the LCA (Sec.5.3) and the reference height for the wind speed is set to h =150 m. The building width normal to the flow is equal to 51 m.

5.1 Input Data for the Analysis

In order to apply the methodology to the case-study building, four wind hazard levels are quantified: very frequent, frequent, occasional and rare. The reference wind speed is taken as the mean hourly wind speed $V_{m,h}$ at $z = h$ (building roof height), representing the wind load intensity measure. The numerical values of the mean wind speed corresponding to 10, 50 and 100 years MRI are determined from the hazard maps reported in the ASCE 7-10 (2010) for Boston (MA). To estimate the wind speed at 1 year MRI the following equation is used (ASCE 2010):

$$V_{TR} = [0.36 + 0.1 \ln(12T_R)]V_{50} \quad (11)$$

where T_R is the return period expressed in years (= 1 year), V_{TR} is the wind speed corresponding to T_R years, and V_{50} is the wind speed corresponding to MRI = 50 year.

The design wind speeds suggested by ASCE 7-10 (2010) represent the 3-sec gust velocity $V_{3\text{-sec}}$, at z = 10 m above the ground, in open terrain. These wind speeds are opportunely converted to mean hourly wind speed, height of the building, and sub-urban terrain (Simiu and Scanlan 1996). Table 1 lists the values of the 3-sec gust from the ASCE 7-10 (2010) for Boston, along with the converted mean hourly wind speeds and the relative MRI.

The coefficients used in the wind load time histories generation are: n = 39, C_z = 10, N_ω = 500, ω_u = 2 rad/s, z_o^{BT} = 0.3 m (suburban terrain), ρ = 1.225 kg/m^3, and C_D = 1.5. The wind direction is along the simulated building axis.

In absence of accurate numerical models, it is assumed that the vortex shedding coming from the adjacent building, which is responsible for the high acceleration levels, can be represented through a sinusoidal gust. The sinusoidal gust is added to the along wind fluctuating force time series and, to simulate the worst case scenario, it is assumed having the same frequency of the structure (equal to 1.2 rad/s) (Cao *et al.* 2016). The gust duration is taken as 150 s, and the gust amplitude is assumed equal to 1.7 m/s to match the acceleration data reported in McNamara *et al.* (2000).

The **M**, **C**, and **K** matrices are constructed using the parameters listed in Cao *et al.* (2016). The total area of the building is taken as 82,612 m^2 (McNamara and Taylor 2003). Considering an average price of US$2,100 per square meter, the initial construction cost, C_0 in Eq. (1), is estimated as US$177.84M. In the LCA analysis, all the other costs will be normalized to C_0. In the Eq. (1),

C_m is taken as the maintenance cost of the dampers, since the costs of structural maintenance would be similar for the building with and without damping system.

5.2 Supplemental Damping

Damper Design

Two different damping strategies are utilized and benchmarked against the building without supplemental damping system, which corresponds to the hypothetical case of the structure without its existing viscous damping system. In the basic performance, the simulated viscous case makes use of the same design parameters of the existing damping scheme (McNamara and Taylor 2003), consisting of 30 fluid viscous dampers, installed every other floor. The damping system is then re-designed to satisfy the essential and the critical performance objectives. The damping coefficients, c_q, are calculated assuming the damping matrix as proportional to stiffness matrix (Connor and Laflamme 2014). The values of the design damping ratio, ξ_d, the corresponding design capacity $F_{\max}$, and number of dampers per floor, N_q, are reported in Table 2 for basic, essential and critical performance objectives.

Additional simulations are conducted with a friction passive device for comparison with the viscous strategy, where the friction dampers are installed at the same locations as the viscous case. In order to design the friction dampers, two criteria are adopted. In the first criterion, the maximum capacity of the friction devices, $F_{\max}$, is determined by equating the energy dissipated by viscous and friction dampers under the design excitation. The values of $F_{\max}$ corresponding to the PBD objectives are listed in Table 2 as Friction-1 case. Fig. 4 (a) shows one realization of the force-displacement loops for the viscous and friction dampers under the frequent wind hazard. In the second criterion, the maximum capacity of the friction devices is set equal to the maximum viscous damper capacity. Table 2 lists the values of the obtained $F_{\max}$ as Friction-2 case and Fig. 4 (b) illustrates the corresponding force-displacement loops.

Simulation of Damping Devices

In the simulations, the damping force, u_v, exerted by a generic viscous dampers is written as:

$$u_v = c \cdot \mathrm{sgn}(\dot{y}) \tag{12}$$

where c is the damping coefficient, $\dot{y}$ is the relative velocity, and $\mathrm{sgn}(\dot{y})$ denotes the sign of $\dot{y}$.

The LuGre friction model is used to simulate the friction force, u_f:

$$u_f = \sigma_0 \zeta + \sigma_1 \dot{\zeta} + \sigma_2 \dot{y} \tag{13}$$

$$\dot{\zeta} = \dot{y} - \sigma_0 \frac{|\dot{y}|}{g(\dot{y})} \zeta \tag{14}$$

where σ_0 is the aggregate bristle stiffness, σ_1 is the microdamping (taken as 0.0017 kN·s·m^{-1}), σ_2 is the viscous friction (taken as 0.0017 kN·s·m^{-1}), ζ is an evolutionary variable, and $\dot{\zeta}$ is its time derivative, $\dot{y}$ is the tangential velocity of the device, and $g(\dot{y})$ is the function that represents the Stribeck effect and is calculated using the following function (Cao *et al.* 2016):

$$g(\dot{y}) = u_c + (u_s - u_c)\exp\left\{-\left(\frac{\dot{y}}{\dot{y}_s}\right)^2\right\} \tag{15}$$

where $\dot{y}_s$ is a constant modeling the Stribeck velocity (taken as 0.002 m·s^{-1}), u_s is the static frictional force, and u_c represents the kinetic frictional force. Here, u_c is taken as the maximum friction force, and u_s is taken as the product of a constant k_1 (taken as 1.065) multiplied by u_c. The maximum friction force u_c is represented by $F_{\max}$ and varies with the PBD target performance level. Table 3 reports the values of σ_0 (Eq. (14)) used in the simulations, that vary nonlinearly with $u_c = F_{\max}$.

5.3 Structural Response

The dynamic analysis is performed by applying the simulated wind load time histories to each floor of the building. As an example, the maximum acceleration profiles for various control cases are reported in Fig. 5 for the wind load corresponding to $V_{m,h}$ = 35 m/s (Fig. 5 a) and $V_{m,h}$ = 41 m/s (Fig. 5 b), and with the damping systems designed to satisfy the basic objective. From Fig. 5, it can be observed that the accelerations reach the maximum values at the last floors of the building. A comparison between the proposed damping strategies shows that Friction-2 dampers (the friction dampers with same maximum capacity of the viscous dampers) provide a better acceleration mitigation than the other two strategies. However, comparing Fig. 5 (a) and (b), one can observe that the damper performance depends highly on the applied wind excitation. In Fig. 5 (a), corresponding to the frequent hazard level, Friction-2 outperforms viscous and Friction-1 in terms of maximum acceleration mitigation. In Fig. 5 (b), corresponding to the occasional hazard level, the performance of Friction-2 is slightly superior to that of the viscous and Friction-1 cases.

Fig. 6 reports the maximum acceleration experienced by the building in the uncontrolled, viscous, Friction-1 and Friction-2 cases for the basic (Fig. 6 (a)), essential (Fig. 6 (b)) and critical (Fig. 6 (c)) design objectives as a function of the wind hazard return period (semi-logarithmic scale). For the basic performance objective, results in Fig. 6 (a) show that without dampers (uncontrolled case) the structure would exceed the acceleration discomfort limits for all the wind hazard levels. The implementation of the designed viscous and friction dampers provides enough mitigation to meet the performance goals for all the considered hazard levels. Figs. 6 (b) and (c) exhibit failure of the uncontrolled case for the essential and critical design objectives, whereas the controlled cases were capable of satisfying all of the performance criteria. Comparing across the examined damping strategies, results demonstrate that Friction-2 outperforms the other strategies in terms of acceleration mitigation for all the hazard levels. Viscous and Friction-1 provide similar acceleration mitigation, as expected due to their similar energy dissipation capabilities.

5.4 Life-cycle Analysis

Vulnerability Analysis

A probabilistic analysis is performed to estimate the probability, $F_j\left(V_{m,h}\right)$, that the maximum acceleration experienced by the structure exceeds a preselected acceleration threshold, conditional on the presence of a mean wind speed $V_{m,h}$. It is assumed that the building will fail when the maximum acceleration of the building is larger than the acceleration threshold corresponding to the *j*-th limit state at least in one of the floors. The considered wind speed, $V_{m,h}$, ranges between $V_{m,h,\min}$ and $V_{m,h,\max}$, taken respectively as 22 and 55 m/s, in order to cover the design velocities reported in Table 1. The function $F_j\left(V_{m,h}\right)$ is expressed as a log-normal function, with log-standard deviation χ_j (shape parameter) and a median μ_j (scale parameter):

$$F_j\left(V_{m,h};\, \chi_j, \mu_j\right) = \Phi\left[\frac{\ln\left(V_{m,h}/\mu_j\right)}{\chi_j}\right] \tag{16}$$

where $\Phi[\cdot]$ is the standard normal distribution function and *j* represents the four limit states. To obtain the values of χ_j and μ_j, a database of structural responses to different $V_{m,h} \in [V_{m,h,\min}, V_{m,h,\max}]$ is created. The database simply contains the maximum acceleration experienced by the building under different levels of wind load with mean wind speed ranging between 22 and 55 m/s. Based on the database results and on the procedure proposed by Shinozuka

et al. (2000), the parameters χ_j and μ_j are determined using the maximum likelihood estimation (MLE) method. To avoid any intersection between the curves, only one value of log-standard deviation (χ_j) is set for all the limit states (Alipour *et al.* 2010). The value for χ is taken as the median value of log-standard deviation χ_j previously estimated with the MLE. The procedure is repeated for all of the control cases. Table 4 lists the estimated log-normal functions parameters. Fig. 7 plots typical conditional exceedance probability curves for uncontrolled, viscous, Friction-1 and Friction-2 cases designed for the basic performance objective. A quick comparison of these curves shows that, for a specific wind hazard intensity, Friction-2 present a lower probability of failure than Friction-1 and viscous.

Hazard Curve

The hazard curve of the wind load depends on the building location. Here, climatological data are obtained from the National Oceanic and Atmospheric Administration (NOAA 2017). A buoy off the coast of Boston, recorded maxima annual wind speeds through an anemometer located at z = 5 m above the buoy surface from 1984 to 2015. The data are converted from open sea to suburban terrain and to mean hourly wind speed at $z = h$ (Simiu and Scanlan 1996). The converted data are subsequently fitted with the MLE method by a three parameter Weibull probability density function to obtain the wind hazard curve, $f(V_{m,h})$:

$$f\left(V_{m,h};\, \eta, \varsigma, \gamma\right) = \frac{\varsigma}{\eta}\left(\frac{V_{m,h}-\gamma}{\eta}\right)^{(\varsigma-1)} \exp\left[-\left(\frac{V_{m,h}-\gamma}{\eta}\right)^{\varsigma}\right] \tag{17}$$

where η is the scale parameter, ς is the shape parameter, and γ is the location parameter of the Weibull distribution, estimated as 3.01, 0.07, and 20.13, respectively.

Expected Acceleration Costs

To apply the LCA procedure, it is necessary to quantify economically the costs C_j (in Eq. (2)) associated with the limit states, as described in Sec. 3.2. Table 5 reports further details regarding the building characteristics.

While there are numerous research indicating a correlation between the building motion and occupant sickness (Mendis *et al.* 2007, Know *et al.* 2015, Lamb *et al.* 2017), a clear mathematical relation between the percentage of building occupants affected by motion sickness and the maximum acceleration experienced by the building is not available in literature. In the absence of

a model to represent the relationship between percentage of building occupants affected by motion sicknesses, ρ_p, and maximum floor acceleration, a_{peak}, the authors assumed four different scenarios, which are illustrated in Fig. 8. In all the cases, the first point corresponds with the assumption *i* of Sec.3.2: ρ_p = 5.4% when a_{peak} > 10 mg. Firstly, the relationship between ρ_p and a_{peak} is assumed linear (Linear-1). Secondly, by the linear interpolation of ρ_p between a_{peak} of 17.5 mg (= middle point of the first acceleration range) and 50 mg (= middle point of the last acceleration range), a second linear function (Linear-2) is obtained, assuming ρ_p equal to 100% (all the floor occupants) when a_{peak} is 50 mg. In the convex case, it is assumed that ρ_p is 70% when a_{peak} is 55 mg and an arbitrary exponential function is fitted to the data. Finally, in concave function, ρ_p is equal to 100% when a_{peak} is 40 mg (= middle point of the medium threshold) and a logarithmic relation is used. One can notice that these scenarios are representative of different levels of severity in the estimation of the percentage of building occupants affected by motion-induced discomfort. For example, the concave function is the most conservative relation, since it assumes that all the building occupants are affected by motion sickness when the peak acceleration is equal to 40 mg. Conversely, Linear-1 is the less conservative, since it assumes that only the 20% of the building occupants will be affected by motion-induced discomfort at high acceleration levels.

The costs C_j are calculated under the above assumptions for the four relationships ρ_p - a_{peak} and for the four limit states. Table 6 lists the C_j values, normalized to the initial construction cost of the building.

5.5 LCA Results and Discussion

The installation cost of the dampers C_I needs to be accounted for in Eq. (1). In the viscous case, C_I is estimated as function of the device maximum capacity, F_{max}, using the following equation (Gidaris and Taflanidis 2012):

$$C_I = 0.77(F_{\max})^{1.207} + 2806 \quad (18)$$

Since the friction devices are generally less expensive than the viscous dampers, their initial cost is estimated as the initial viscous cost reduced by 30%. In addition, an installation cost of $10,000 for the supportive bracing system of each damper is considered (Laflamme 2011). No maintenance costs are included (data available in Taylor Devices 2017), thus C_m = 0. A summary of the device costs of the viscous and friction dampers is reported in Table 7 as a function of the design objective.

The table includes the bracing system costs and the device costs normalized the building initial construction cost.

From the convolution of fragility functions (Eq. (16)) and wind hazard curves (Eq. (17)), the annual probability of failure, P_j in Eq. (3), is obtained. Fig. 9 summarizes the steps required for the failure cost estimation, in the case of viscous dampers designed for the basic performance objective and convex function. Applying the four proposed relationships ρ_p - a_{peak}, the failure costs, C_f, are computed for the uncontrolled building and for the dampers designed to respect the basic, essential and critical design objectives schematized in Fig. 1. The failure costs are normalized to C_0, and summarized in Table 8 and Fig. 10.

Results in Table 8 show the dependence of the C_f on the assumed ρ_p - a_{peak} relationship, independently on the pursued design objective. More specifically, when the percentage of building occupants affected from motion sickness (ρ_p) is high (e.g., concave relationship), the cost benefits due to the integration of damping devices are amplified.

The LCC of the structure equipped with damping devices is computed with Eq. (1). Fig. 11 illustrates bar plots of LCC for the basic, essential, and critical design, with concave ρ_p - a_{peak} relationship, normalized to the initial construction cost. The LCC of the uncontrolled building is assumed as target cost. Results in Fig. 11 demonstrate that all the designed damping systems satisfy the target cost check (Fig. 2). A comparison between the LCC of different control strategies shows that the basic performance objective leads to the lowest saving in comparison with the uncontrolled building. In the essential case, both viscous and Friction-2 strategies allow higher saving than Friction-1. Finally, when the dampers are designed for the critical performance objective, the benefits arising from the wind-induced acceleration mitigation highly overcome the target cost, yielding to significant savings over the lifetime of the structure. The critical design results the most economically convenient, in spite of the highest initial installation costs due to the high capacity of the devices. The viscous strategy yielded better financial performance compared with the Friction-1 case, but to lower mitigation than Friction-2.

6. Conclusions

This paper provided the framework for a performance-based design (PBD) methodology for passive damping systems integrated in tall buildings. Target performance levels in terms of maximum acceptable accelerations are introduced and related to different wind hazard levels. The

wind hazard is probabilistically characterized by return periods of the mean wind speed. The passive dampers are sized to satisfy three performance objectives: basic, essential and critical. A life-cycle analysis (LCA) is integrated in the PBD procedure to quantify the economic benefits of the damping devices over the life span of the structure. The failure costs are related to the percentage of building occupants potentially affected by motion sickness.

The PBD is applied to a 39-story building, located in Boston (MA), subjected to boundary layer winds. The wind speed is simulated as a multivariate stochastic process, in the time domain. Numerical simulations are conducted to evaluate the structural response of the building under different wind hazards. Three control strategies are investigated: viscous dampers, friction dampers with equivalent dissipated energy, and friction dampers with equivalent capacity to that of viscous devices. The dampers are designed to meet the accelerations requirements associated with basic, essential and critical performance objectives. An LCA is conducted to assess the benefits of the control strategies over the lifetime of the structure. The life-cycle cost (LCC) of the building equipped with the designed dampers is calculated, and it is used to compare the financial effectiveness of the three control strategies. Results showed that, between the considered passive strategies, the friction damping is the most economically effective. In particular, it allows relevant saving when the devices are designed for the critical objective. The investigations presented in this paper are based on the assumptions that the wake excitation coming from neighbor building can be represented with a sinusoidal gust, and that the relations between percentage of building occupants affected by motion sickness and maximum acceleration follows linear, concave and convex functions. These assumptions were made by the authors in absence of more accurate numerical models.

This preliminary investigation demonstrated that the proposed PBD procedure is promising at estimating the potential economic benefits of the integration of passive damping systems in tall buildings. Future work will include the use of a more realistic model for the wind load and probabilistic evaluation of motion control systems performance. In addition, a wind directionality-study will be initiated, which will provide additional information to the damping system designer.

Acknowledgement

This paper is based upon work supported by the National Science Foundation under Grant No. 1537626. Their support is gratefully acknowledged. Any opinions, findings, and conclusions or

recommendations expressed in this material are those of the authors and do not necessarily reflect the views of the National Science Foundation.

Appendix A. Spectral approach for wind load time series simulation

In this paper the quasi-steady model is employed for the generation of the along-wind drag force, expressed as:

$$F_j(t) = 0.5\,\rho\,C_D A_j\left[V_{m,j} + V_{t,j}(t)\right]^2 \chi_D(f) \cong \rho\,C_D A_j V_{m,j} V_{t,j}(t)\,\chi_D(f) \tag{A.1}$$

where the term $0.5\,\rho\,C_D A_j {V_{t,j}}^2(t)$ is negligible as it is very small in comparison with the other components, and only the dynamic component of the wind load is considered, since the objective of the dampers implementation is the reduction of the dynamic wind-induced effects. In Eq. (A.1), ρ indicates the air density, C_D is the drag coefficient, A_j is the area of the building normal to the wind flow at the *j*-th floor, $V_{m,j}$ is the mean component of the wind speed at the *j*-th floor, $V_{t,j}(t)$ is the fluctuating component of the wind velocity at the *j*-th floor, and χ_D^2 is the aerodynamic admittance function for drag which is a function of frequency *f*, assumed equal to 1, according to the quasi-static condition. The spectral approach is used to simulate the fluctuating wind speed caused by the wind turbulence, which is denoted by $V_{t,j}(t)$ (Shinozuka and Deodatis 1991, Deodatis 1996). For a *n*-story building, the power spectral density matrix, $\mathbf{S}(\omega)$, can be written as:

$$\mathbf{S}(\omega) = \begin{bmatrix} S_{11}(\omega) & \cdots & S_{1n}(\omega) \\ \vdots & \ddots & \vdots \\ S_{n1}(\omega) & \cdots & S_{nn}(\omega) \end{bmatrix} \tag{A.2}$$

where ω is the frequency (rad/s), and elements of the $\mathbf{S}(\omega)$ matrix are expressed as:

$$S_{ji} = \begin{cases} s_j(\omega), & j = i \\ \sqrt{s_j(\omega) s_i(\omega)}\,\gamma_{ji}(\omega), & j \neq i \end{cases} \tag{A.3}$$

where $s_j(\omega)$ is the Kaimal power spectral density function, and γ_{ji} is the following coherence function between the turbulence at the *j*-th and *i*-th floors, at heights z_j and z_i:

$$\gamma_{ji}(\omega) = \exp\left[-\frac{\omega}{2\pi}\,\frac{C_z|z_j - z_i|}{\frac{1}{2}\left(V_{m,j} + V_{m,i}\right)}\right] \tag{A.4}$$

where C_z is the correlation coefficient. The Kaimal power spectral density function, $s_j(\omega)$, is expressed as (Simiu and Scanlan 1996):

$$s_j(\omega) = \frac{200}{2\pi} u_*^2 \frac{z}{V_{m,j}} \frac{1}{\left(1 + 50\ \frac{\omega z}{2\pi V_{m,j}}\right)^{5/3}} \tag{A.5}$$

where u_* is the friction velocity of the wind flow, equal to:

$$u_* = \frac{0.4 V_{m,j}}{\ln(z/z_o^{BT})} \tag{A.6}$$

where z_o^{BT} is the roughness of the building situ. Using the Cholesky decomposition, the power spectral density matrix $\mathbf{S}(\omega)$ is decomposed into:

$$\mathbf{S}(\omega) = \mathbf{H}(\omega)\mathbf{H}^{\mathrm{T}*}(\omega) \tag{A.7}$$

where the asterisk denotes the complex conjugate and $\mathbf{H}(\omega)$ is a lower triangular matrix of the form:

$$\mathbf{H}(\omega) = \begin{bmatrix} H_{11}(\omega) & \cdots & 0 \\ \vdots & \ddots & \vdots \\ H_{n1}(\omega) & \cdots & H_{nn}(\omega) \end{bmatrix} \tag{A.8}$$

The fluctuating wind velocity time history $V_{t,j}$ at a generic floor *j* is obtained as superposition of trigonometric functions with random phase angles (Deodatis 1996):

$$V_{t,j}(t) = 2 \sum_{m=1}^{n} \sum_{l=1}^{N_\omega} \left|H_{jm}(\omega_{ml})\right| \sqrt{\Delta\omega} \cos[\omega_{ml} t - \vartheta_{ml}(\omega_{ml}) + \Phi_{ml}] \tag{A.9}$$

where *m* and *l* are two indices, $\Delta\omega$ represents the frequency step amplitude, equal to ω_u / N_ω, where ω_u is the cut-off frequency and N_ω is the number by which the frequency domain is divided, ω_{ml} is equal to:

$$\omega_{ml} = l\Delta\omega - \frac{m-l}{m}\Delta\omega \tag{A.10}$$

Φ_{ml} is a sequence of random numbers from the uniform distribution in the range [0, 2π], and ϑ_{ml}:

$$\vartheta_{ml}(\omega) = \tan^{-1}\left\{\frac{\mathrm{Im}\left[H_{jm}(\omega_{ml})\right]}{\mathrm{Re}\left[H_{jm}(\omega_{ml})\right]}\right\} \tag{A.11}$$

where Im[·] and Re[·] denote imaginary and real quantities, respectively.

References

Alipour, A., Shafei, B., & Shinozuka, M. (2010). Performance evaluation of deteriorating highway bridges located in high seismic areas. . *Journal of Bridge Engineering*, 597-611.

Architectural Institure of Japan. (2004). AIJ-GEH-2004. *Maruzen Publishing*.

ASCE 7-10. (2010). *Minimum Design Loads for Buildings and Other Structures.* 1801 Alexander Bell Drive, Reston, Virginia 20191: ASCE Standard, ASCE/SEI 7-10. American Society of Civil Engineers.

Bernardini, E., Spence, S. M., Kwon, D. K., & Kareem, A. (2014). *Performance-based design of high-rise buildings for occupant comfort.* Journal of Structural Engineering.

Biondini, F., & Frangopol, D. M. (2009). Lifetime reliability-based optimization of reinforced concrete cross-sections under corrosion. *Structural safety*.

Burns, S. A. (2002). *Recent advances in optimal structural design.* ASCE Publications.

Burton, M. D., Kwok, K. C., & Abdelrazaq, A. K. (2015). Wind-induced motion of tall buildings: designing for occupant comfort. *International Journal of High-Rise Buildings*.

Cao, L., Laflamme, S., Taylor, D., & Ricles, J. . (2016). Simulations of a Variable Friction Device for Multihazard Mitigation. *Journal of Structural Engineering*.

Chuang, W. C., & Spence, S. M. (2017). A performance-based design framework for the integrated collapse and non-collapse assessment of wind excited buildings. *Engineering Structures*.

Ciampoli, M., Petrini, F., & Augusti, G. (2011). Performance-based wind engineering: towards a general procedure. *Structural Safety*.

Connor, J., & Laflamme, S. (2014). *Structural motion engineering.* Springer.

Cui, W., & Caracoglia, L. . (2015). Simulation and analysis of intervention costs due to wind-induced damage on tall buildings. *Engineering Structures*, 183-197.

Deodatis, G. (1996). Simulation of ergodic multivariate stochastic processes. *Journal of engineering mechanics*, 778-787.

Federal Emergency Management Agency (FEMA). (2012). *Seismic performance assessment of buildings, Volume 1 - Methodology.* Washington, DC: FEMA Pubblication P-58-1.

Griffis, L., Patel, V., Muthukumar, S., & Baldava, S. (2013). A framework for performance-based wind engineering. *Advances in Hurricane Engineering: Learning from Our Past* .

Hou, F., & Sarkar, P. P. (2018). A time-domain method for predicting wind-induced buffeting response of tall buildings. . *Journal of Wind Engineering and Industrial Aerodynamics*.

Huang, M. F., Li, Q., Chan, C. M., Lou, W. J., Kwok, K. C. S., & Li, G. (2015). Performance-based design optimization of tall concrete framed structures subject to wind excitations. *Journal of Wind Engineering and Industrial Aerodynamics*, 70-81.

Ierimonti, L., Caracoglia, L., Venanzi, I., & Materazzi, A. L. . (2017). Investigation on life-cycle damage cost of wind-excited tall buildings considering directionality effects. *Journal of Wind Engineering and Industrial Aerodynamics*.

Jackson, M., & Scott, D. M. (2010). Increasing efficiency in tall buildings by damping. *Structures Congress* , 3132-3142.

Kareem, A., Kijewski, T., & Tamura, Y. (1999). Mitigation of motions of tall buildings with specific examples of recent applications. *Wind and structures*, 201-251.

Kwok, K. C., Burton, M. D., & Abdelrazaq, A. K. . (2015). Wind-induced motion of tall buildings: designing for habitability. . *American Society of Civil Engineers*.

Kwok, K. C., Hitchcock, P. A., & Burton, M. D. (2009). Perception of vibration and occupant comfort in wind-excited tall buildings. . *Journal of Wind Engineering and Industrial Aerodynamics*.

Laflamme, S. . (2011). *Control of large-scale structures with large uncertainties.*

Laflamme, S., Taylor, D., Abdellaoui Maane, M., & Connor, J. J. . (2012). Modified friction device for control of large-scale systems. *Structural control and health monitoring*, 548-564.

Lamb, S., & Kwok, K. C. S. . (2016). Sopite syndrome in wind-excited buildings: productivity and wellbeing impacts. *Building Research & Information*, 1-12.

Lamb, S., & Kwok, K. C. S. (2017). The fundamental human response to wind-induced building motion. *Journal of Wind Engineering and Industrial Aerodynamics*.

Lamb, S., Kwok, K. C. S., & Walton, D. . (2014). A longitudinal field study of the effects of wind-induced building motion on occupant wellbeing and work performance. *Journal of wind engineering and industrial aerodynamics*, 39-51.

Li, G., & Hu, H. . (2014). Risk design optimization using many-objective evolutionary algorithm with application to performance-based wind engineering of tall buildings. *Structural Safety*.

Liew, J. R., Tang, L. K., & Choo, Y. S. . (2002). Advanced analysis for performance-based design of steel structures exposed to fires. *Journal of Structural Engineering*.

Mcnamara, R. J., & Taylor, D. P. (2003). Fluid viscous dampers for high-rise buildings. . *The structural design of tall and special buildings*, 145-154.

McNamara, R. J., Huang, C. D., & Wan, V. . (2000). Viscous-damper with motion amplification device for high rise building applications. *Proceedings of the 2000 Structures Congress & Exposition*, 1-10.

Mendis, P., Ngo, T., Haritos, N., Hira, A., Samali, B., & Cheung, J. (2007). Wind loading on tall buildings. *EJSE Special Issue: Loading on Structures*, 41-54.

Moehle, J., & Deierlein, G. G. (2004). A framework methodology for performance-based earthquake engineering. *13th world conference on earthquake engineering* .

Moon, K. S. (2010). Vertically distributed multiple tuned mass dampers in tall buildings: performance analysis and preliminary design. *The Structural Design of Tall and Special Buildings*.

National occupational employment and wage estimates united states. (2015). *United States Department of Labor* .

NOAA. (2017). Retrieved from http://www.ndbc.noaa.gov/

Petrini, F., & Ciampoli, M. (2012). Performance-based wind design of tall buildings. *Structure and Infrastructure Engineering*.

Porter, K. A. (2003). An overview of PEER's performance-based earthquake engineering methodology. *Proceedings of Ninth International Conference on Applications of Statistics and Probability in Civil Engineering*.

Rossi, R., Lazzari, M., & Vitaliani, R. (2004). Wind field simulation for structural engineering purposes. . *International journal for numerical methods in engineering*, 738-763.

Saaed, T. E., Nikolakopoulos, G., Jonasson, J. E., & Hedlund, H. . (2015). A state-of-the-art review of structural control systems. *Journal of Vibration and Control*.

Shinozuka, M., & Deodatis, G. . (1991). Simulation of stochastic processes by spectral representation. . *Applied Mechanics Reviews*, 191-204.

Shinozuka, M., Feng, M. Q., Lee, J., & Naganuma, T. . (2000). Statistical analysis of fragility curves. . *Journal of engineering mechanics*, 1224-1231.

Simiu, E., & Scanlan, R. H. (1996). *Wind effects on structures.* Wiley.

Spence, S. M., & Gioffrè, M. . (2012). Large scale reliability-based design optimization of wind excited tall buildings. *Probabilistic Engineering Mechanics*.

Spence, S. M., & Kareem, A. (2014). Performance-based design and optimization of uncertain wind-excited dynamic building systems. *Engineering Structures*.

Taflanidis, A. A., & Beck, J. L. . (2009). Life-cycle cost optimal design of passive dissipative devices. *Structural Safety*, 508-522.

Tamura, Y., & Kareem, A. (2013). *Advanced structural wind engineering.* Springer Science & Business Media.

Tamura, Y., Kawana, S., Nakamura, O., Kanda, J., & Nakata, S. (2006). Evaluation perception of wind-induced vibration in buildings. *Proceedings of the Institution of Civil Engineers-Structures and Buildings,*.

Taylor Devices. (2017). Retrieved from http://www.seismicdamper.com/

Tse, K. T., Kwok, K. C., & Tamura, Y. . (2012). Performance and cost evaluation of a smart tuned mass damper for suppressing wind-induced lateral-torsional motion of tall structures. *Journal of Structural Engineering*.

Tubaldi, E., Barbato, M., & Ghazizadeh, S. . (2012). A probabilistic performance-based risk assessment approach for seismic pounding with efficient application to linear systems. *Structural Safety*.

Ubertini, F., & Giuliano, F. . (2010). Computer simulation of stochastic wind velocity fields for structural response analysis: comparisons and applications. *Advances in Civil Engineering*.

Van de Lindt, J. W., & Dao, T. N. . (2009). Performance-based wind engineering for wood-frame buildings. . *Journal of Structural Engineering*.

Wang, L., Zhao, X., & Zheng, Y. M. . (2016). A combined tuned damper and an optimal design method for wind-induced vibration control for super tall buildings. *The Structural Design of Tall and Special Buildings*.

Wen, Y. K., & Kang, Y. J. (2001). Minimum building life-cycle cost design criteria. I: Methodology. *Journal of Structural Engineering*.

Yang, T. Y., Moehle, J., Stojadinovic, B., & Der Kiureghian, A. (2009). Seismic performance evaluation of facilities: methodology and implementation. *Journal of Structural Engineering*.

Appendix A. Spectral approach for wind time series simulation

The spectral approach is used to simulate the fluctuating wind speed caused by the wind turbulence, which is denoted by $V_{t,j}(t)$ (Shinozuka and Deodatis 1991, Deodatis 1996). In this approach, the fluctuating wind velocity is simulated as a multivariate ergodic stochastic process. For a *n*-story building, the power spectral density matrix, $\mathbf{S}(\omega)$, can be written as:

$$\mathbf{S}(\omega) = \begin{bmatrix} S_{11}(\omega) & \cdots & S_{1n}(\omega) \\ \vdots & \ddots & \vdots \\ S_{n1}(\omega) & \cdots & S_{nn}(\omega) \end{bmatrix} \quad \text{(A.1)}$$

where ω is the frequency (rad/s), and elements of the $\mathbf{S}(\omega)$ matrix are expressed as:

$$S_{ji} = \begin{cases} s_j(\omega), & j = i \\ \sqrt{s_j(\omega) s_i(\omega)}\, \gamma_{ji}(\omega), & j \neq i \end{cases} \tag{A.2}$$

where $s_j(\omega)$ is the Kaimal power spectral density function, and γ_{ji} is the following coherence function between the turbulence at the *j*-th and *i*-th floors, at heights z_j and z_i:

$$\gamma_{ji}(\omega) = \exp\left[-\frac{\omega}{2\pi}\frac{C_z|z_j - z_i|}{\frac{1}{2}\left(V_{m,j} + V_{m,i}\right)}\right] \tag{A.3}$$

where C_z is the correlation coefficient. The Kaimal power spectral density function, $s_j(\omega)$, is expressed as (Simiu and Scanlan 1996):

$$s_j(\omega) = \frac{200}{2\pi} u_*^2 \frac{z}{V_{m,j}} \frac{1}{\left(1 + 50\,\frac{\omega z}{2\pi V_{m,j}}\right)^{5/3}} \tag{A.4}$$

where u_* is the friction velocity of the wind flow, equal to:

$$u_* = \frac{0.4 V_{m,j}}{\ln(z/z_o^{BT})} \tag{A.5}$$

where z_o^{BT} is the roughness of the building situ. Using the Cholesky decomposition, the power spectral density matrix $\mathbf{S}(\omega)$ is decomposed into:

$$\mathbf{S}(\omega) = \mathbf{H}(\omega)\mathbf{H}^{\mathrm{T}*}(\omega) \tag{A.6}$$

where the asterisk denotes the complex conjugate and $\mathbf{H}(\omega)$ is a lower triangular matrix of the form:

$$\mathbf{H}(\omega) = \begin{bmatrix} H_{11}(\omega) & \cdots & 0 \\ \vdots & \ddots & \vdots \\ H_{n1}(\omega) & \cdots & H_{nn}(\omega) \end{bmatrix} \tag{A.7}$$

The fluctuating wind velocity time history $V_{t,j}$ at a generic floor j is obtained as superposition of trigonometric functions with random phase angles (Deodatis 1996):

$$V_{t,j}(t) = 2\sum_{m=1}^{n}\sum_{l=1}^{N_\omega}\left|H_{jm}(\omega_{ml})\right|\sqrt{\Delta\omega}\cos[\omega_{ml}t - \vartheta_{ml}(\omega_{ml}) + \Phi_{ml}] \quad \text{(A.8)}$$

where m and l are two indices, $\Delta\omega$ represents the frequency step amplitude, equal to ω_u/N_ω, where ω_u is the cut-off frequency and N_ω is the number by which the frequency domain is divided, ω_{ml} is equal to:

$$\omega_{ml} = l\Delta\omega - \frac{m-l}{m}\Delta\omega \quad \text{(A.9)}$$

Φ_{ml} is a sequence of random numbers from the uniform distribution in the range [0, 2π], and ϑ_{ml}:

$$\vartheta_{ml}(\omega) = \tan^{-1}\left\{\frac{\mathrm{Im}\left[H_{jm}(\omega_{ml})\right]}{\mathrm{Re}\left[H_{jm}(\omega_{ml})\right]}\right\} \quad \text{(A.10)}$$

where Im[·] and Re[·] denote imaginary and real quantities, respectively.

Table 1 Wind speed values for the 39-story building in Boston.

MRI (years)	$V_{3\text{-sec}}$ **(m/s)**	$V_{m,10}$ **(m/s)**	$V_{m,h}$ **(m/s)**
1	27.0	14.0	25.0
10	36.0	19.0	35.0
50	45.0	23.0	41.0
100	48.0	25.0	44.0

Table 2 Design parameters for viscous and friction devices.

Performance objective	ξ_d	**Floor**	**Viscous**	**Friction-1**	**Friction-2**	N_q
			F_{max} **(kN)**	F_{max} **(kN)**	F_{max} **(kN)**	
Basic	2 %	above 26th floor	45	31	45	2
		below 26th floor	90	62	90	2
Essential	6 %	above 26th floor	271	100	271	2
		below 26th floor	133	200	133	2
Critical	18 %	above 26th floor	404	267	404	2
		below 26th floor	814	578	814	2

Table 3 Friction damper parameter σ_0 used in the simulations.

F_{max} **(kN)**	σ_0 **(kN/m)**
< 45	1.75×10^4
53 - 62	4.20×10^4
90 - 111	7.00×10^4
222 - 267	1.57×10^5
404	2.80×10^5
814	7.00×10^5

Table 4 Parameters of the conditional probability curves for basic, essential and critical design.

Performance objective	**Control strategy**	**Scale parameter** μ				**Shape parameter** χ
		Negligible	**Minor**	**Medium**	**Extreme**	
Basic	Uncontrolled	3.10	3.20	3.30	3.36	0.165
	Viscous	3.16	3.25	3.31	3.37	0.132
	Friction-1	3.18	3.27	3.31	3.35	0.127
	Friction-2	3.23	3.27	3.33	3.37	0.113
Essential	Viscous	3.23	3.33	3.37	3.38	0.094
	Friction-1	3.27	3.33	3.38	3.38	0.074
	Friction-2	3.29	3.35	3.37	3.40	0.070
Critical	Viscous	3.33	3.38	3.46	0*	0.074
	Friction-1	3.35	3.38	3.43	0*	0.055
	Friction-2	3.37	3.42	0*	0*	0.052

* the limit state is never exceeded

Table 5 Building characteristics and other parameters used in the LCA.

LCA Parameter	Value
Floor area	2,090 m^2
Total number of employees	15,300
Number of employees per floor	425
Number of employees on the top third floors	5,100
Average annual salary	US$112,500
Average salary/day	US$477
Economic loss from sick employees/day	30.1%US$477=US$143

Table 6 Annual economic losses associated with different ρ_p - a_{peak} relationships for the acceleration thresholds, normalized to the initial construction cost.

Limit state	Linear-1	Linear-2	Concave	Convex
Negligible	0.27 %	0.27 %	0.27 %	0.27 %
Minor	0.54 %	2.06 %	3.30 %	0.71 %
Medium	0.76 %	3.49 %	4.92 %	1.56 %
Extreme	0.98 %	4.92 %	4.92 %	3.44 %

Table 7 Total installation cost of viscous and friction devices as function of the performance objective, normalized to the initial construction cost.

Performance objective	Viscous	Friction-1	Friction-2
Basic	0.21%	0.20 %	0.20 %
Essential	0.22 %	0.21 %	0.21 %
Critical	0.25 %	0.22 %	0.23 %

Table 8 Failure costs for uncontrolled and controlled building with dampers designed respectively for basic, essential and critical performance, normalized to the initial construction cost.

Performance objective	Control strategy	Failure cost, C_f			
		Linear-1	Linear-2	Concave	Convex
Basic	Uncontrolled	4.46 %	17.01 %	22.19 %	9.05 %
	Viscous	4.12 %	15.92 %	20.66 %	8.53 %
	Friction-1	4.11 %	16.13 %	20.65 %	8.78 %
	Friction-2	3.75 %	14.75 %	19.03 %	7.91 %
Essential	Viscous	3.08 %	11.87 %	15.08 %	6.56 %
	Friction-1	4.11 %	16.13 %	20.67 %	8.78 %
	Friction-2	2.66 %	10.36 %	13.32 %	5.61 %
Critical	Viscous	0.87 %	2.27 %	3.42 %	1.02 %
	Friction-1	1.19 %	3.92 %	5.75 %	1.74 %
	Friction-2	0.62 %	1.55 %	2.32 %	0.72 %

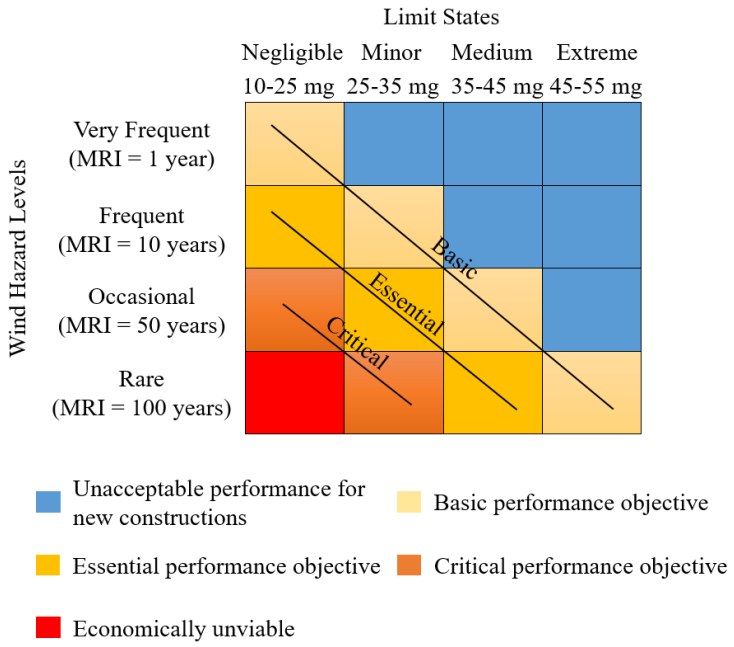

Figure 1 PBD matrix for wind hazard: wind hazard levels and acceptable acceleration ranges.

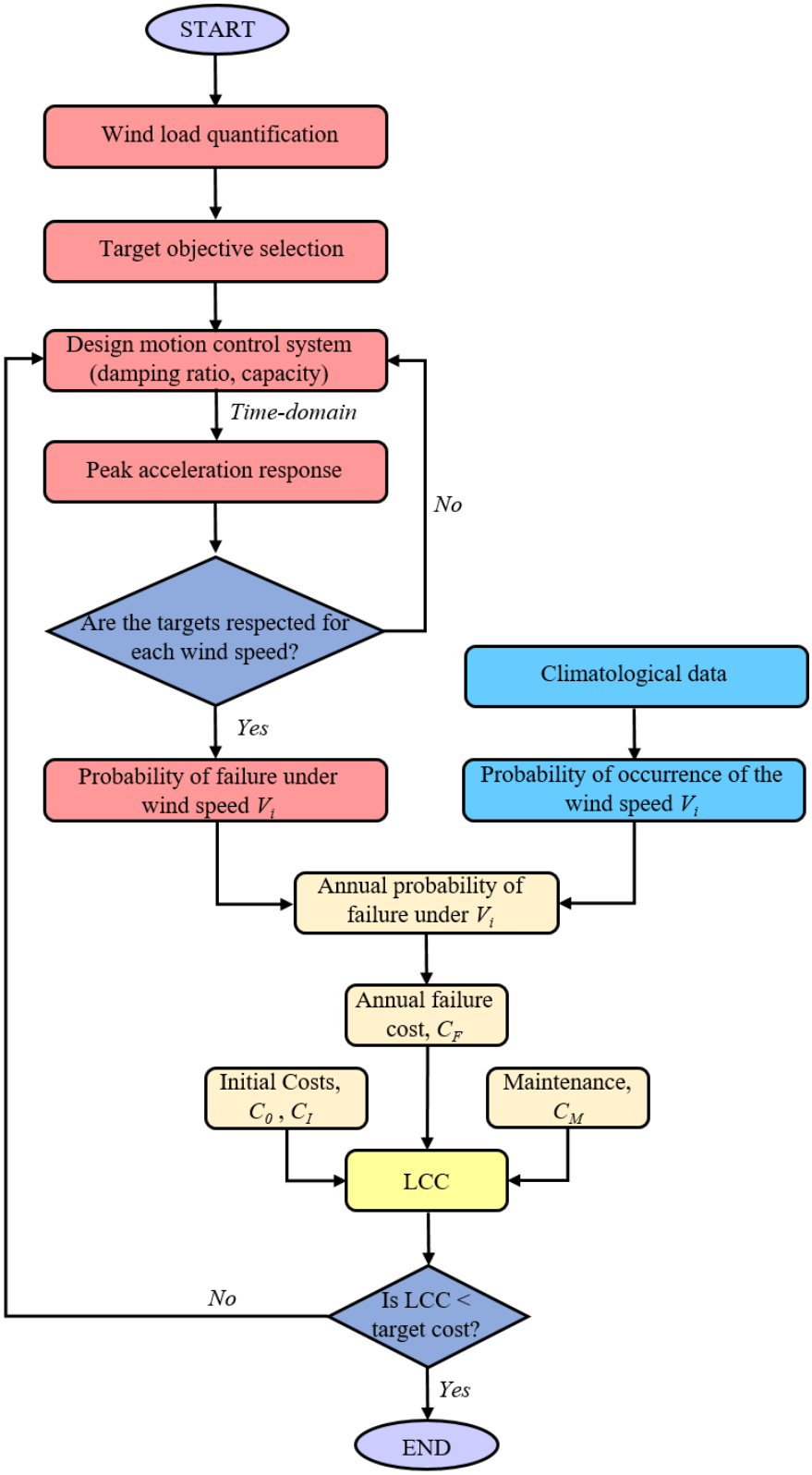

Figure 2 Damper design and life-cycle analysis flow-chart.

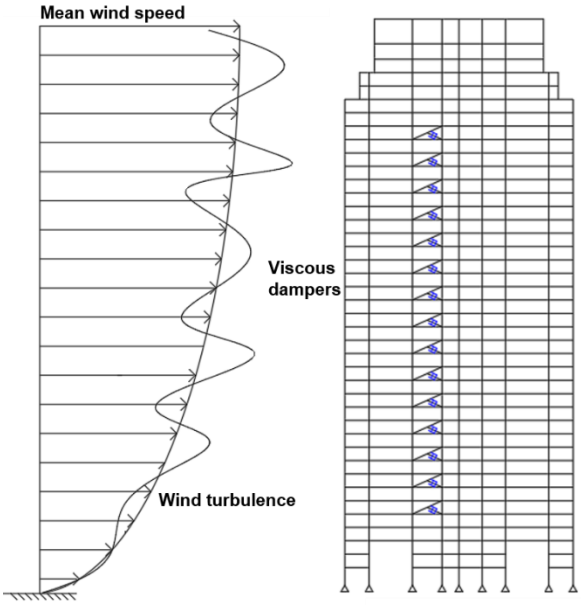

Figure 3 Schematic representation of the wind loads, along with the building elevation in the simulated direction (not in scale).

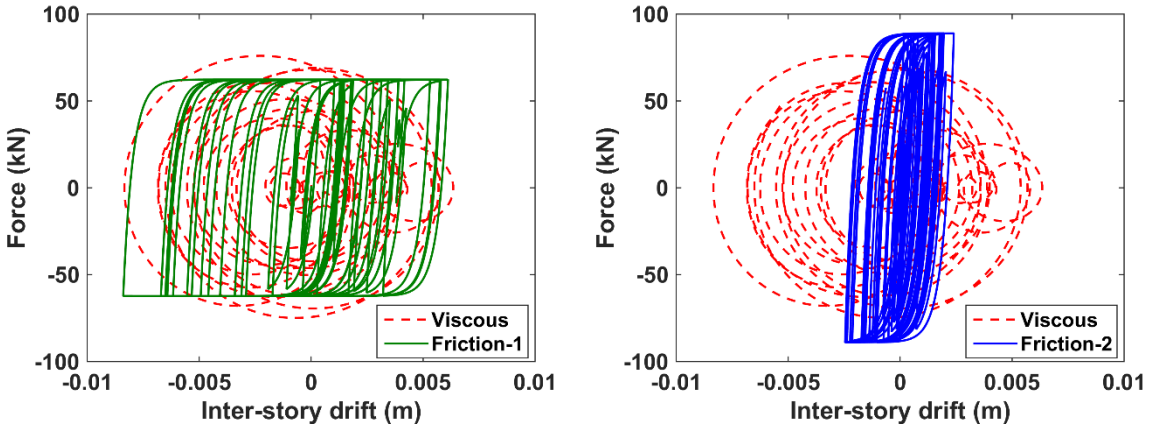

(a) (b)

Figure 4 Force-displacement loops for viscous and friction dampers with: (a) different capacity, but equal dissipated energy (Friction-1 case), (b) same capacity (Friction-2 case).

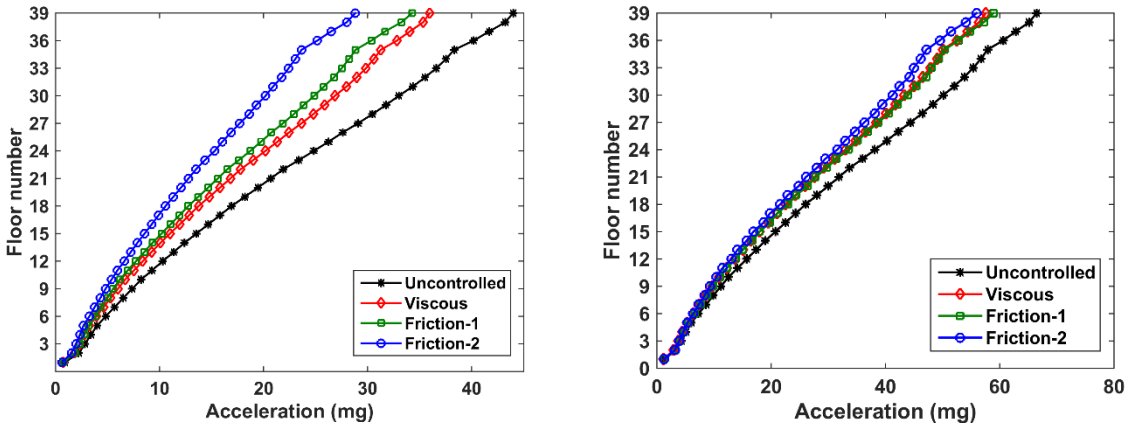

Figure 5 Maximum acceleration experienced by the structure equipped with dampers designed for the basic performance objective for (a) $V_{m,h}$ = 35 m/s (frequent hazard level) and (b) for $V_{m,h}$ = 41 m/s (occasional level).

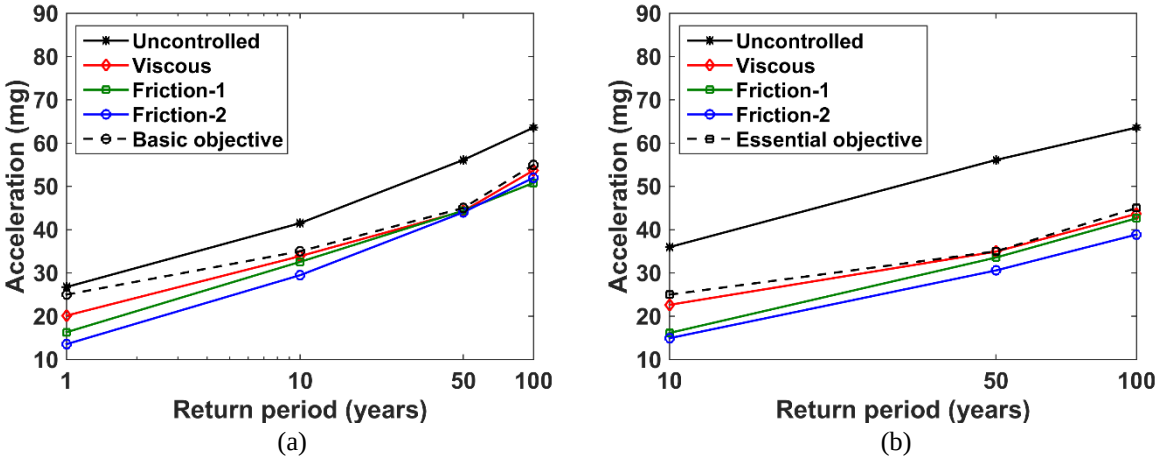

(a)

(b)

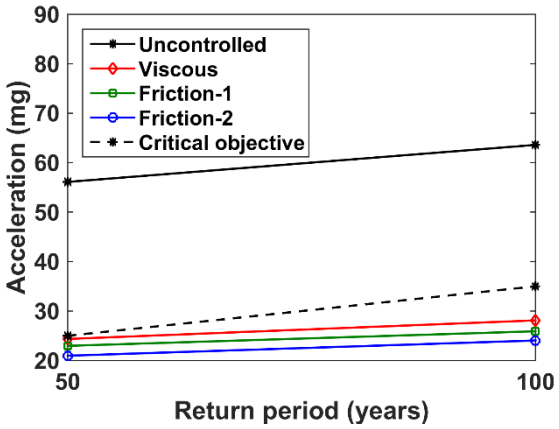

(c)

Figure 6 Maximum acceleration experienced by the uncontrolled and controlled buildings with dampers designed for (a) basic (b) essential (c) critical design performance objectives.

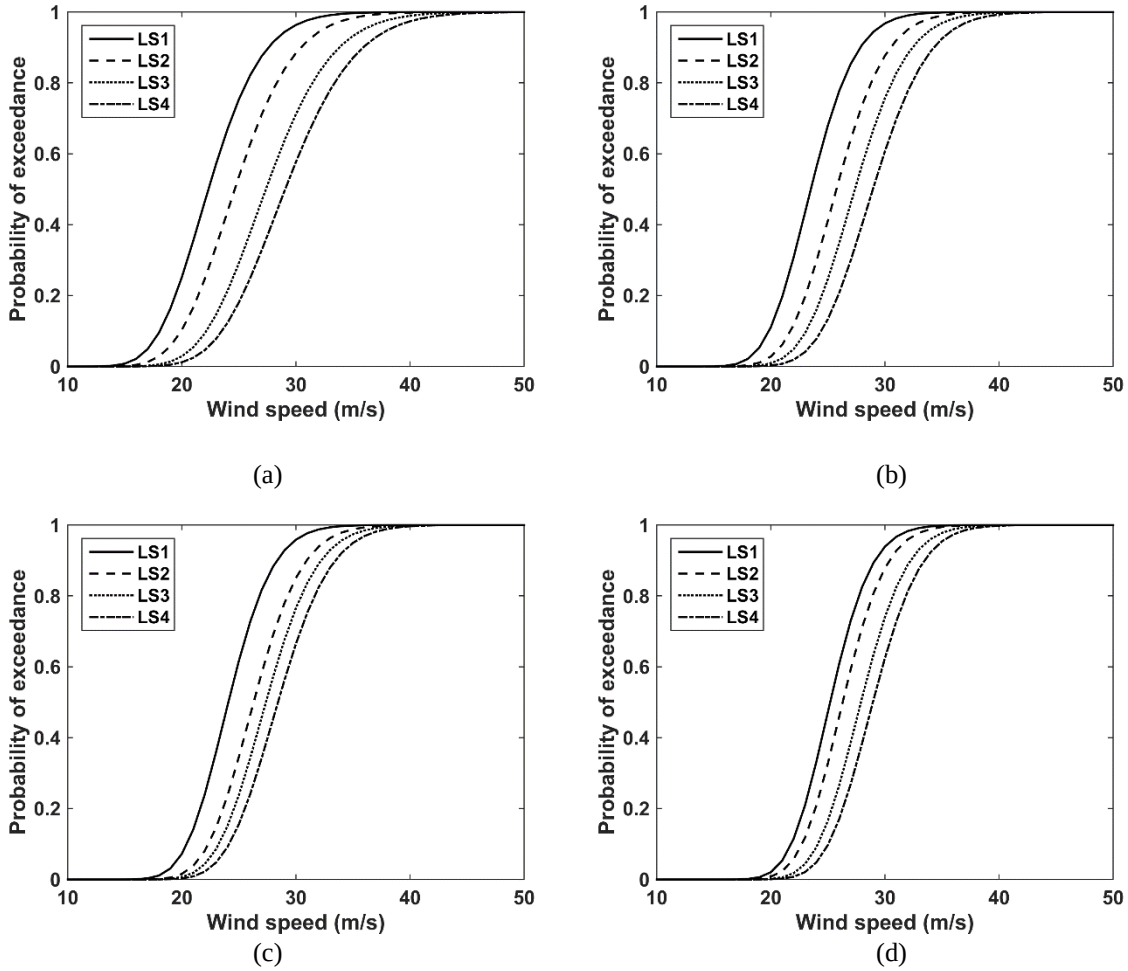

Figure 7 Conditional exceedance probability of the peak acceleration for the four limit states (LS): (a) uncontrolled building, (b) building equipped with viscous dampers, (c) Friction-1, (d) Friction-2.

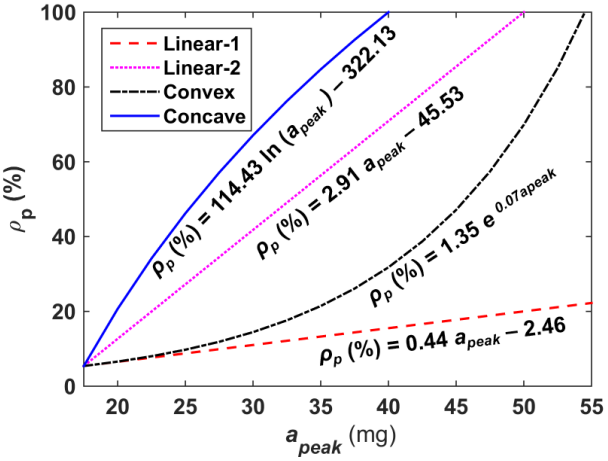

Figure 8 Proposed relationships between peak acceleration and percentage of building occupants affected by wind-induced discomfort and motion sickness.

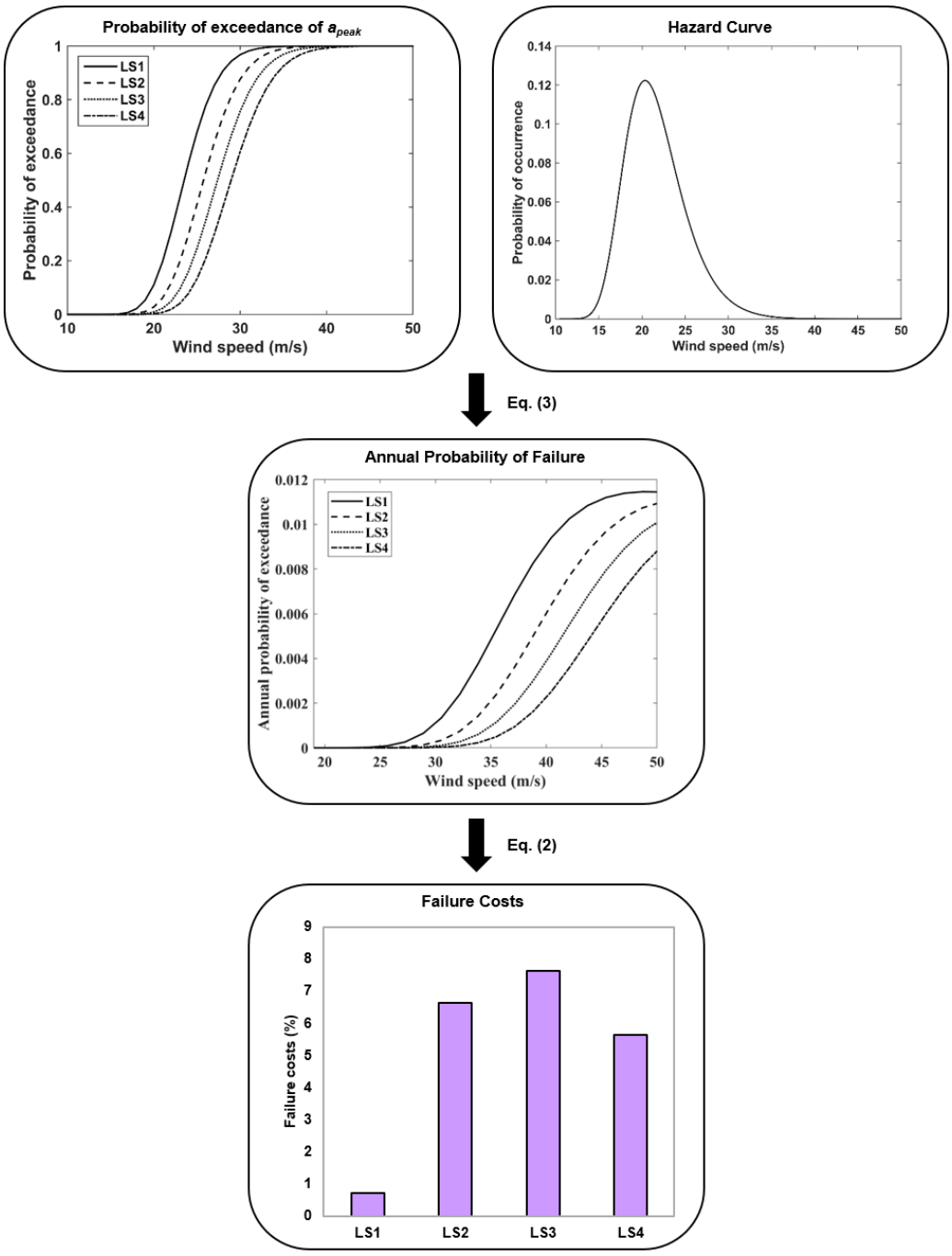

Figure 9 Summary of the required steps for the estimation of the failure costs divided for limit states (LS) in the case of viscous dampers, designed with the basic performance objective, and using the convex relation. The failure costs are normalized to the initial construction cost.

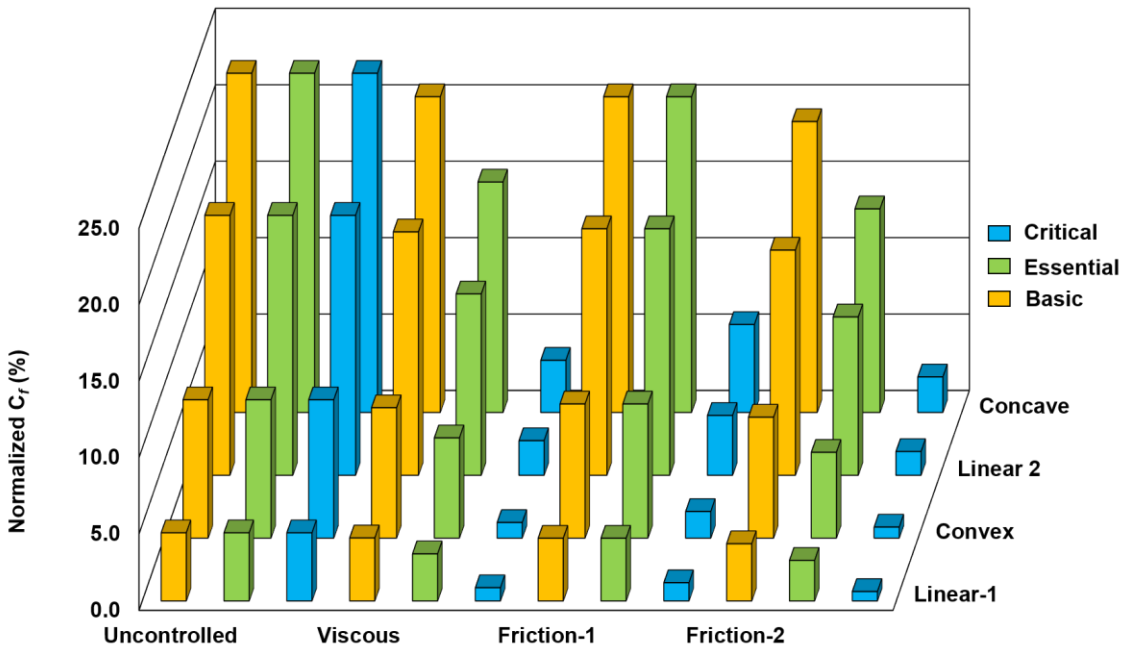

Figure 10 Failure costs normalized to the initial construction cost in the cases of uncontrolled and controlled buildings, with dampers designed for basic, essential, and critical performance objectives and for the four percentage of building occupants-maximum acceleration.

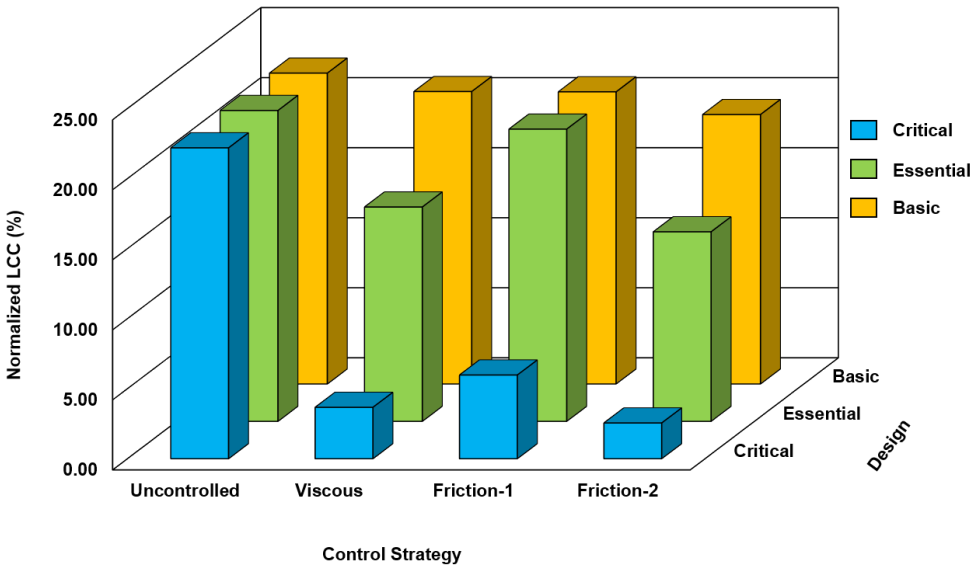

Figure 11 LCC normalized to the initial construction cost taking the concave relationship in the cases of uncontrolled and controlled buildings, with dampers designed for basic, essential, and critical performance objectives.